Protein Science (1998), 7:1671–1680. Cambridge University Press. Printed in the USA.

Improving the binding affinity of an antibody using molecular modeling and site-directed mutagenesis

CLAYTON L. CASIPIT,[1] RONY TAL,[1] VAUGHAN WITTMAN,[1] PIERRE-ANDRÉ CHAVAILLAZ,[2] KATHY ARBUTHNOTT,[2] JON A. WEIDANZ,[2] JIN-AN JIAO,[3] AND HING C. WONG[1]

[1]Department of Molecular Biology, Sunol Molecular Inc., 2173 NW 99th Avenue, Miami, Florida 33172
[2]Department of Immunology, Sunol Molecular Inc., 2173 NW 99th Avenue, Miami, Florida 33172
[3]Department of Protein Chemistry, Sunol Molecular Inc., 2173 NW 99th Avenue, Miami, Florida 33172

(RECEIVED March 23, 1998; ACCEPTED May 14, 1998)

Abstract

Activated Factor X releases F1.2, a 271-amino acid peptide, from the amino terminus of prothrombin during blood coagulation. A nine-amino acid peptide, C9 (DSDRAIEGR), corresponding to the carboxyl terminus of F1.2 was synthesized and used to produce a monoclonal antibody, TA1 (K_D 1.22×10^{-6} M). To model the TA1 antibody, we entered the sequence information of the cloned TA1 F_v into the antibody modeling program, ABM, which combines homology methods, conformational search procedures, and energy screening and has proved to be a reliable and reproducible antibody modeling method. Using a novel protein fusion procedure, we expressed the C9 peptide fused to the carboxyl terminus of the PENI repressor protein from *Bacillus licheniformis* in *Escherichia coli*. We constructed fusion proteins containing alanine substitutions for each amino acid in the C9 epitope. Binding studies, using the C9 alanine mutants and TA1, and spatial constraints predicted by the modeled TA1 binding cleft enabled us to establish a plausible conformation for C9 complexed with TA1. Furthermore, based on binding results of conservative amino acid substitutions in C9 and mutations in the antibody, we were able to refine the complex model and identify antibody mutations that would improve binding affinity.

Keywords: affinity improvement; computer modeling; peptide–antibody complex; site-directed mutagenesis

There have been several X-ray crystallographic studies of antigen–antibody complexes that have revealed much about interactions that occur at the binding interface between antibodies and their antigens (for reviews, see Braden & Poljak, 1995; Searle et al., 1995). These complexes can be separated into different groups based on the reactive antigens within the complexes. The antibody complexes studied include those with haptens or small chemical structures (Herron et al., 1989; Brunger et al., 1991), peptides (Stanfield et al., 1990; Rini et al., 1992; Schulze-Gahmen et al., 1993), proteins (Amit et al., 1986; Braden et al., 1994), DNA (Herron et al., 1991), and antibodies themselves in idiotype–antiidiotype complexes (Bentley et al., 1990; Ban et al., 1994; Evans et al., 1994). Once contact residues are identified by X-ray crystallography, some studies further examine the binding interactions by creating point mutations in the antibody or antigen and assaying for changes in affinity. Verdaguer et al. (1995) utilized peptide epitopes with specific point mutations to identify key interacting residues and provided molecular interpretation for those interactions seen in the X-ray–resolved complex model. Another group studying a hapten–antibody complex used molecular modeling to dock the hapten into the X-ray–resolved antibody structure, then mutated key residues in the antibody to verify the docked model (Strong et al., 1991).

Modeling procedures to predict structure for antibodies of known sequence but unknown structure have been developed using X-ray resolved antibodies entered in the Brookhaven database (Bruccoleri et al., 1988; Chothia et al., 1989; Rees et al., 1992). In two hapten–antibody studies that employed antibody modeling techniques, potential interacting residues within the antibody binding cleft were identified from the antibody model and verified by site-directed mutagenesis (Near et al., 1993; Ruff-Jamison & Glenney, 1993). A protein–antibody study used a predicted antibody structure to dock a hen egg lysozyme epitope of a known structure and then mutated predicted antibody contact residues within the complex model and used the binding results to refine the model (de la Paz et al., 1986; Roberts et al., 1987). Other groups have used information about protein–protein recognition and the forces that drive complex formation to develop algorithms based on surface complementarity and energy scoring to predict antigen–antibody docking (Walls & Sternberg, 1992; Totrov & Abagyan, 1994). Although their methods used predicted or determined antibody structures as docking targets, they still assumed prior knowledge of the epitope conformation.

Reprint requests to: Clayton L. Casipit, Iconix Pharmaceuticals, 850 Maude Ave., Mountain View, California 94043; e-mail: ccasipit@mail.iconixpharm.com.

A common factor exists in all these modeling studies: the antigenic determinants were of known or easily predictable structures, either haptens (small molecules with a limited number of conformations) or peptide epitopes from X-ray resolved crystallized proteins. To date, no studies involving peptide–antibody complex determinations have attempted to model the complexed structure of an antibody and its peptide epitope strictly through site-directed mutational analysis and computational means.

Here, we present our work in which a nine-amino acid linear epitope, C9 (Degan et al., 1983), of unknown structure was folded and docked into its modeled antibody, TA1, using only computer modeling and binding information from mutations made in either the epitope or the antibody. We introduced scanning alanine mutations in the C9 epitope using a novel protein fusion method (R. Tal, C.L. Casipit, V. Wittman, H.C. Wong, in prep.), which involves fusing the C9 peptide to the carboxyl terminus of the PENI repressor protein from *Bacillus licheniformis* (Wittman & Wong, 1988) and expressing it in *Escherichia coli*. Using the binding information from these C9 mutations along with the spatial constraints of the modeled TA1 binding cleft, we were able to establish a plausible model for the C9–TA1 complex. With binding information from further mutations within C9 and TA1, we refined the model and were able to identify specific mutations in TA1 that would improve affinity.

Results

General characteristics and quality of the antibody model

Based on the lengths of the light chain CDRs the TA1 combining site topography can be described as a cavity or groove, which are characteristic of antibodies that bind haptens and peptides (Wang et al., 1991). We ran Procheck (Laskowski et al., 1993), which checks the stereochemical quality of protein structures, on the final TA1 antibody model. The resulting Ramachandran plot showed 81.3% of the residues to be in the most energetically favored regions with 3% (six residues) being in generously allowed or disallowed regions. Three of these aberrant residues are within heavy chain and three are within light chain. Chothia et al. (1989) found, through the alignment of structurally resolved antibodies, that CDRs can be grouped into canonical classes based on specific amino acids within the CDR loops that define a secondary structure. To determine if any of the six aberrant residues defined a canonical class and thus played a pivotal role in determining the binding site topography, we aligned the TA1 sequence to those of the canonically grouped antibodies. We also examined the TA1 model to determine if these residues are positioned in or near the combining site where docking with C9 could be significantly affected. We found that one of the aberrant residues, Met56 in L2, was directly adjacent to Arg55, a residue forming a key hydrogen bond with C9 in the proposed docking model. The aberrant residue could affect how Arg55 is placed and, therefore, affect how C9 is docked in this portion of the cleft. All other aberrant residues were either in regions distant from the combining site or in a region where the amino acid sequence was nearly identical to an X-ray resolved canonical loop, therefore having no significant affect on the backbone CDR loop placement. So, although the Ramachandran plot statistics imply the antibody model is not of high quality, further examination would indicate that most of the aberrant residues have no significant affect on the backbone CDR loop placement within the combining site. To ensure that no side chains were penetrating the binding site surface, the minimized antibody model was also checked for intra-molecular bumping. No significant bumping was revealed. However, it should be noted that these computational analyses indicate very little about the accuracy of the side-chain positions. Therefore, we cannot be completely sure of the binding site topography. Nevertheless, because there are no obvious problems with the CDR loop backbones and the minimized structure shows no penetrating side chains in the binding site surface, we feel the antibody model is a reasonable structure for us to attempt to use as a docking constraint.

Alanine substitutions in C9 (fine epitope mapping)

Each of the positions in C9 were substituted with alanine with the exception of Ala5, which was replaced with Ser. The SDS electrophoresis and Western analysis for the mutant purified PENI–C9 fusion proteins are shown in Figure 1. Competition EIA and BIAcore results are presented in Table 1. The three sets of binding assay results follow similar trends when relative binding is compared. The assays demonstrate that when either Ile6, Gly8, or Arg9 are substituted with Ala, binding is decreased or eliminated compared to wild type C9. When Glu7 is substituted with Ala, binding is increased compared to wild-type C9 or increased compared to any of the other mutations. To determine if the carboxy terminus interacts with the TA1 binding cleft, we also performed competition EIA on a chemically modified C9 peptide that contained a carboxy terminal amide group instead of a hydroxyl. This chemically synthesized modification did not bind with TA1 (data not shown). These results indicated that the residues in the carboxy terminal half of C9, XXXXAIXGR, had the greatest influence in TA1 binding. Furthermore, Glu7 had to be positioned in such a way that substitution of the side chain with the smaller, aliphatic one of Ala would make the binding interaction at the interface more favorable. We used this information to dock the C9 epitope into the modeled TA1 binding cleft.

The initial antigen–antibody complex model

The initial modeled complex was consistent with the affinity results from the alanine-scanning mutagenesis and was identical to the final refined model (see Figs. 2–7), with the following two exceptions. (1) Arg9 side chain was more linear and formed only one hydrogen bond with Arg55 in L2. (2) The carboxyl group at

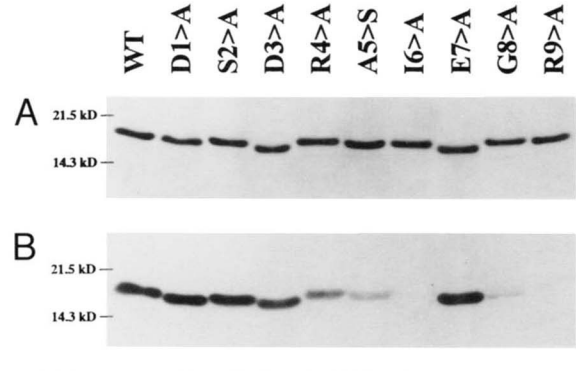

Fig. 1. Purity and affinity to TA1 of the PENI–C9 scanning alanine mutants. **A:** SDS-PAGE of PENI–C9 wild type and mutants; 1 μg per lane. **B:** Western analysis of PENI–C9 wild type and mutants.

Table 1. *Relative binding data for the PENI–C9 proteins*

Mutation	Competition EIA[a]	BIAcore[b]
Wild type	50	100
D1A	64	51
S2A	49	48
D3A	39	51
R4A	2	36
A5S	4	34
I6A	8	9
E7A	82	63
G8A	11	45
R9A	8	21
AAAAAIAGR	74	105
R9K	1	1
R9I	7	0.1
E7Q	88	96
E7D	46	58
E7K	94	113
I6L	19	43
I6V	19	64
A5G	13	34
A5C	27	7
R4K	43	
D1&3N	69	
D1W	74	
S2W	59	
D3W	44	
D1P	63	

[a]Reported as percent inhibition of maximum EIA signal.
[b]Reported as percent of relative response of PENI–C9 wild type.

the carboxy terminus formed a hydrogen bond with Tyr213 in H3. Both of these characteristics of the initial model were consistent with the binding knockout observed when Arg9 was substituted with Ala and when the carboxy terminus hydroxyl was replaced with an amide group.

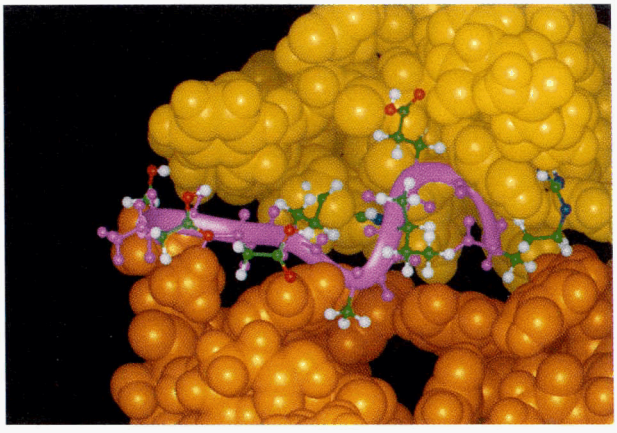

Fig. 3. C9–TA1 complex. C9 is shown with its α-carbon backbone rendered as a ribbon and side chains as ball and stick. The TA1 framework regions have been removed.

Refining the complex model: Additional C9 mutations and mutations in TA1

The complexed model provided the information necessary to devise other mutations in C9 with which we could test the positioning of the C9 residues and derive how the key residues may interact at the C9/TA1 interface. Specifically, the residues we chose to test in C9 were Arg9 (possible side-chain hydrogen bond), Glu7 (side chain is positioned between L3 and L1), Ile6 (side chain possibly excludes water), Ala5 (possible α-carbon backbone amine hydrogen bond), Arg4 (possible side chain hydrogen bond), Asp3, Ser2, and Asp1 (side chains are free of any interaction with TA1). The SDS electrophoresis and Western Blot results for these residue substitutions are shown in Figures 8 and 9. There is a higher molecular weight protein (40 kDa) detected for a few of the samples in the Western Blot in Figure 8B. We believe this to be dimer formed as a result of these particular mutations; we have also observed this attribute in earlier purified samples of PENI that

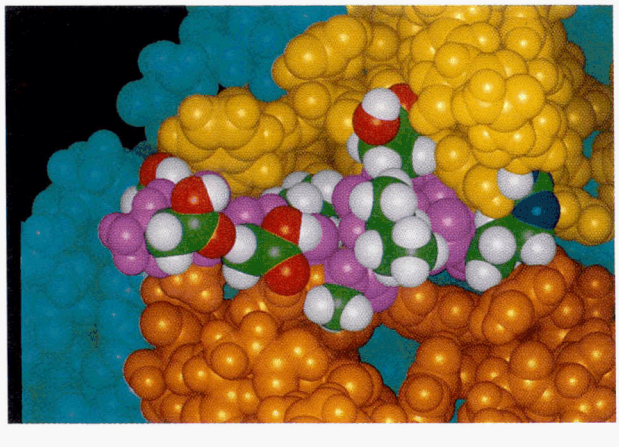

Fig. 2. Space-filling rendering of the C9 epitope docked into the TA1 binding cleft. C9 is shown with its α-carbon backbone (mauve) and side chains: carbon (green), oxygen (red), nitrogen (blue), and hydrogen (white). The TA1 antibody is shown with its framework regions (cyan), light-chain CDR regions (yellow), and heavy chain CDR regions (orange).

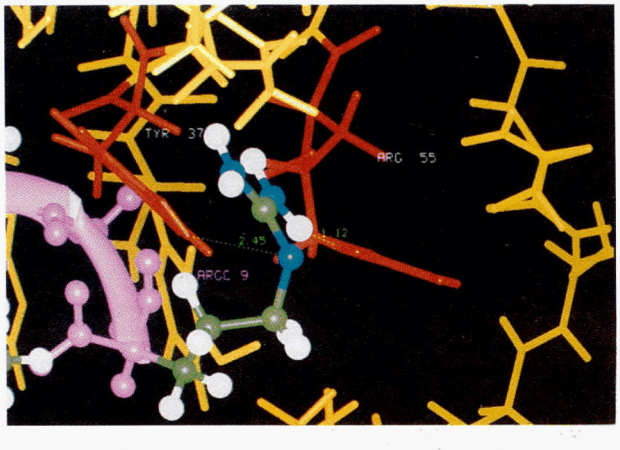

Fig. 4. Two hydrogen bonds occur between TA1 and Arg9 side chain in C9. A hydrogen bond (1.12 Å) occurs between Arg55 in TA1 L2 and an amine group in the Arg9 side chain. A second hydrogen bond (2.45 Å) occurs between Tyr37 in TA1 L1 and the amide group in the Arg9 side chain. The interacting residues in TA1 are colored red.

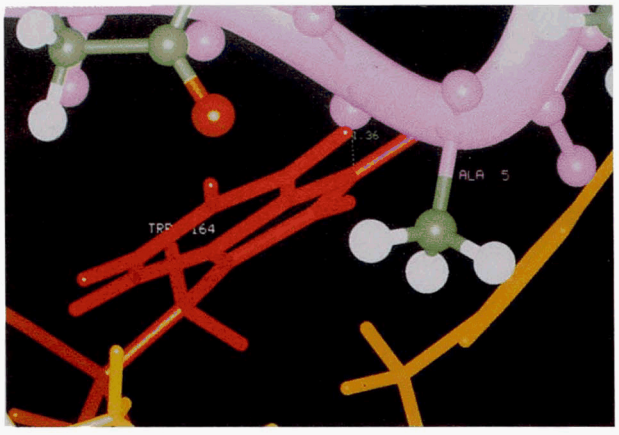

Fig. 5. A hydrogen bond (1.36 Å) occurs between Trp164 in TA1 H2 (red) and the backbone amine at Ala5 in C9.

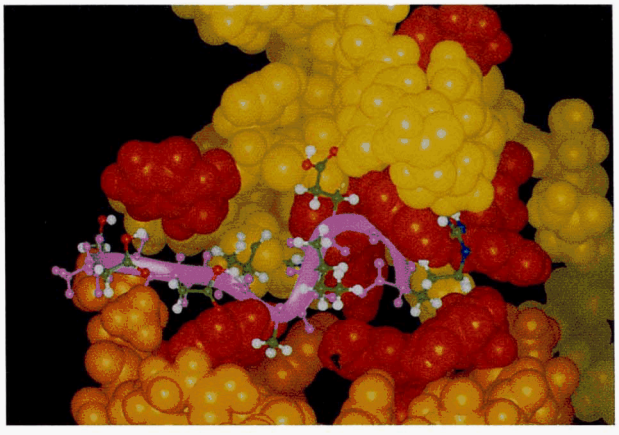

Fig. 7. Mutated positions (red) in the TA1 antibody. In the light chain, Leu 30 in L1 (at the top), Phe99 in L3 (far left), His96 in L3 (center), Tyr37 in L1 (right center), and Arg55 in L2 (far right). In the heavy chain, Trp164 in H2 (left), Tyr213 in H3 (center), and Tyr218 in H3 (right).

have been stored for a time. Competition EIA and BIAcore results are presented in Table 1. The binding results of the mutations relative to each other compare well except in the case of the Ala5Cys mutation. The Western blot and competition EIA results show a similar trend for this mutation but the BIAcore results indicate very low binding. When performing the Western blot, we found that the Ala5Cys mutation band could only be detected when the blot was probed in the presence of 100 mM DTT. Therefore, we believe the Cys mutation may be causing disulfide bonds to form, blocking the epitope from binding to TA1 and preventing detection by BIAcore.

In addition to mutations in C9 we also devised mutations within the TA1 antibody to test the model's accuracy and improve antibody affinity. We targeted residues that were predicted from the model to interact with C9 or to form the binding site topography of TA1. These residues were Arg55 in L2 (possibly hydrogen bonded with Arg9), Tyr213 in H3 (possibly hydrogen bonded with the carboxy terminus), Tyr37 in L1 (in close proximity to C9), Trp164 in H2 (possibly hydrogen bonded with Ala5), and His96 in L3 (possibly hydrogen bonded with Arg4). Leu30 in L1, Phe99 in L3, and Tyr218 in H3 were chosen as experimental controls. These mutated antibodies were assayed for binding to C9 using BIAcore (Fig. 10). Arg55, Tyr213, Tyr37, Trp164, and His96 appear to contribute to the binding site topography because when substituted with Ala to produce a radical change in side chain volume, binding to C9 is significantly reduced. The binding results for all the TA1 mutations were consistent with what the model depicted except for the Tyr37Phe and Tyr213Phe mutations, in which side-chain volume is maintained while the potential hydrogen bonding group is removed. We did not expect the lower affinity seen for Tyr37Phe because this residue was predicted to be close to C9 but have no

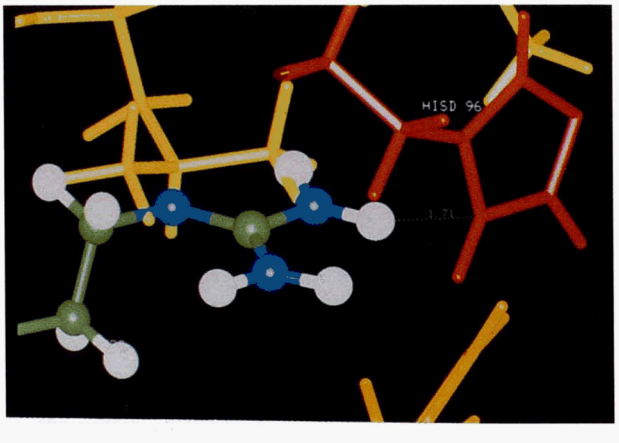

Fig. 6. A hydrogen bond (1.71 Å) occurs between His96 in TA1 L3 (red) and the Arg4 side chain in C9.

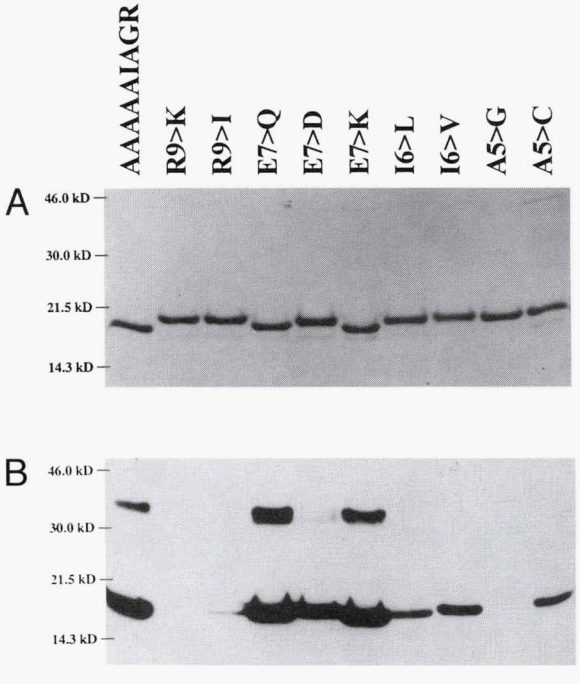

Fig. 8. Purity and affinity to TA1 of the additional PENI–C9 mutants. **A:** SDS-PAGE of PENI–C9 mutants; 1 μg per lane. **B:** Western analysis of PENI–C9 mutants.

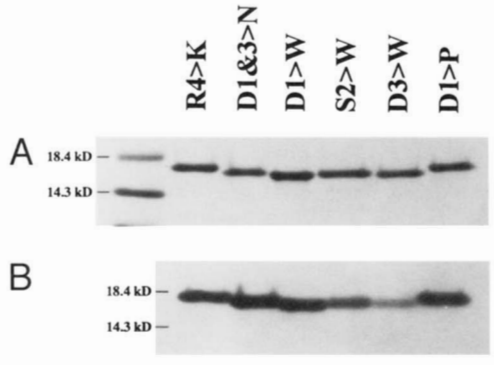

Fig. 9. Purity and affinity to TA1 of the additional PENI–C9 mutants. **A:** SDS-PAGE of PENI–C9 mutants; 1 μg per lane. **B:** Western analysis of PENI–C9 mutants.

hydrogen bond interaction. We did expect a lower affinity for Tyr213Phe due to a predicted Tyr213 hydrogen bond with the carboxy terminus, but found increased affinity. These results led us to refine the model.

Final refinement of the antigen–antibody complex

To refine the model to fit the binding results, the C9 epitope needed to be adjusted in such a way as to form a hydrogen bond with Tyr37 and to remove the hydrogen bond between Tyr213 and the C9 carboxy terminus while still maintaining the other hydrogen bonds and the overall C9 α-carbon backbone conformation. To achieve this, the C9 epitope was translated approximately 0.1 Å along the *y*-axis toward the light chain, thus breaking the Tyr213–carboxy terminal hydrogen bond. The dihedral angles of the atom bonds along the Arg9 side chain and α-carbon were modified and when the side chain was adjusted to lie closer to the C9 α-carbon backbone, the Arg9 side chain formed a second hydrogen bond with Tyr37. All other existing interactions remained essentially the same. The final refined complexed model is described below.

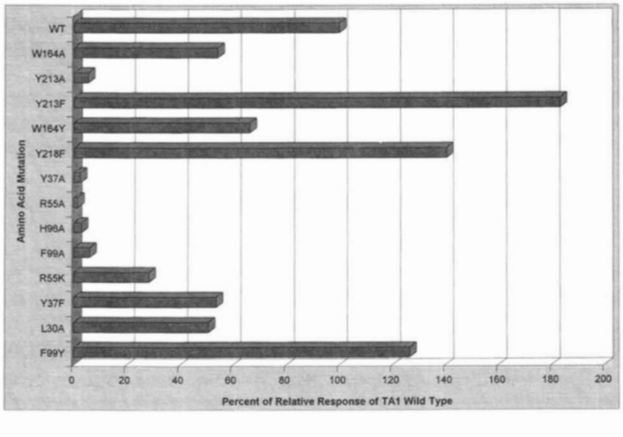

Fig. 10. BIAcore (relative binding) results of TA1 wild type and mutants.

Discussion

Reliability of the complex model

Ideally, the way to test the accuracy of a modeled antigen–antibody complex is to analyze the atomic structure by X-ray crystallography. Instead, we attempted to use site-directed mutagenesis to test and refine the model. Specific mutations were made either in the C9 peptide or in the binding interface of the TA1 antibody. These resulted in changes in affinity which correlated with the structure of the modeled antigen–antibody complex.

The modeled C9 epitope was examined for conformity with general structural characteristics observed in other antigenic peptides of known structure. The C9 peptide does not appear to interact with the binding cleft as an extended linear structure. It must take on a structured β-turn form to fit into the cleft, thus implying that this peptide may have a preference for a particular conformation as is consistent with many short antigenic peptide epitopes (for review, see Dyson & Wright, 1995). Also, the Ramachandran plot of the C9 model structure that we propose shows that the residues fall within the energetically allowed regions, indicating the backbone geometry is of reasonable quality. Furthermore, there is no significant VDW violations within C9 or at the binding interface with TA1. However, there is a space gap at the interface, between the H3–H2 loops of TA1 and the middle of C9 (see Figs. 2, 3). A possible explanation for this is that this area may be closed off by H3 during complex formation.

The scanning alanine mutations and the combined alanine mutant (AAAAA**AI**A**GR**) of the C9 peptide indicate that the Ala5, Ile6, Gly8, and Arg9 residues are integral for C9 binding to TA1. The affects of TA1 antibody mutations Tyr37Phe and Arg55Lys indicate that Tyr37 and Arg55 in the light chain are important for TA1 binding to C9. These observations correlate with the final refined model and are presented below in the context of other binding results to describe the positioning of each C9 residue and its interactions with the TA1 binding cleft.

Hydrogen bond interactions between Arg9 side chain in C9 and Tyr37 in L1 and Arg55 in L2 are important in the overall binding of TA1 to C9 (see Fig. 4)

This is supported by the affects of mutations in both the C9 peptide and the TA1 antibody. In C9, all mutations at the Arg9 position reduce binding. Even replacement with the most conservative amino acid, Lys, which preserves side chain charge and most of the volume, still nearly eliminates binding. The TA1 antibody Tyr37Phe mutation results in a 50% reduction in affinity, and Arg55Lys mutation results in a 70% reduction in affinity. Both mutations conserve overall volume but change chemical groups on the side chains that are predicted to participate in hydrogen bonding with Arg9. These residues fall within L1 and L2 in positions, which are highly variable among structurally defined antibodies (Chothia et al., 1989). Thus, the results imply that these residues are crucial for the specificity of TAl; they are not located at positions that define the canonical loop structure, but are instead located at positions that are highly variable and are occupied by amino acids that have hydrogen bond acceptor and donor groups (Jeffrey & Saenger, 1991). In addition to hydrogen bonding, a favorable electrostatic interaction could also occur between the -NH group of the Arg9 side chain of C9 and the aromatic ring face of Tyr37 (Creighton, 1993).

Gly8 does not directly interact with the antibody but is integral for C9 recognition

The Gly8Ala mutation in C9 results in a large reduction in binding. Spatial restrictions within the binding cleft may require the C9 α-carbon backbone to take on a sharp bend at this position, requiring a dihedral angle that is only allowed by Gly (Schulz & Schirmer, 1979). Although the side chain of Ala is slightly larger than that of Gly, this mutation is not tolerated, implying that the binding cleft surrounding this position has a spatial constraint that will fit only the smaller side chain of Gly. In the model, the binding cleft space occupied by Gly reflects these observations.

Glu7 also does not directly interact with the antibody

Depicted in the model, the Glu side chain lies in a crease running between L3 and L1 (see Figs. 2, 3). At this position the side chain lies outside of the spatial constraints of the cleft. This is consistent with the binding results for the peptides with changes at this position. The Ala substitution decreases side chain volume and removes charge, the Gln substitution conserves side chain volume and neutralizes charge, and the Lys substitution increases side chain volume and changes charge. All result in unchanged binding, implying that radical volume changes or changes in charge at this position are tolerated because of lack of surrounding spatial restriction. The Asp mutation, which decreases side chain volume but conserves negative charge, results in decreased binding, implying that a possible charge repelling affect or bumping may be present when the side chain is constrained closer to the C9 backbone.

Ile6 may play a conformational role in the C9 backbone

The Ala substitution indicates Ile6 is one of the key positions. It is not likely the Ile side chain participates in a hydrogen bond because it has an aliphatic side chain (Jeffrey & Saenger, 1991) but it is possible that this hydrophobic side chain serves to repel water from the interacting surfaces. However, if this were the only function, one would expect to see equivalent binding when this position was mutated to Leu, which conserves side chain volume, and decreased binding when mutated to Val, which decreases side chain volume. Western and BIAcore analysis results show the opposite; Val binds better than Leu. Comparison of the branching pattern of each of these aliphatic side chains shows that Val, which branches at the C_β atom, more closely resembles the Ile side chain structure than Leu, which branches at the C_γ atom. The C_β-branched side chain serves to stiffen the main chain more than the C_γ side chain of Leu (Schulz & Schirmer, 1979). So the Ile side chain may act to hold the C9 backbone in the proper conformation.

Ala5 side chain may also play a conformational role (see Fig. 5)

The binding results for the C9 peptide containing mutations at the Ala5 position are ambiguous, particularly in the case of the Cys mutation. As discussed earlier in Results, this could be the effect of disulfide bond formation in the BIAcore assay. The Ser and Cys mutations, which mimic Ala side chain volume closely, show some binding, while the Gly mutation, which reduces side chain volume, eliminates binding. To investigate the potential of a hydrogen bond between the Ala backbone amine and Trp164 in H2 in TA1, we made the Trp164Tyr mutation in TA1. Although this mutation conserves some volume, it removes the predicted hydrogen bonding partner and resulted in reduced binding. The position of Trp164 is not a canonical structure determinant for H2 but it is located at the junction between H2 and FR2 and may define a take-off angle of the H2 loop from the framework and would influence combining site topography. Therefore, it is difficult to design other mutations to adequately test the possibility of the hydrogen bond.

Arg4 side chain forms a possible hydrogen bond interaction with His96 in L3 (see Fig. 6)

The C9 mutations to Ala or Lys at position 4 resulted in a 50 and 10% decrease in binding, respectively. This would indicate that the predicted hydrogen bond interaction contributes only partially to the affinity. The His96Ala mutation in L3 in TA1 resulted in binding knockout. This result may be due to perturbation of the loop conformation rather than to the modification of an antigen contact residue. His96 is in a canonical loop-defining region and is adjacent to a primary residue that defines canonical class. A conservative mutation, such as Lys or Arg, at this position may reveal more about the possible role of this residue; however, it is difficult to adequately test the possibility of the hydrogen bond.

Asp1, Ser2, and Asp3 are positioned in free space within the binding cleft

The scanning alanine mutations and the combined alanine mutant in C9 all demonstrate that these three residues at the amino terminus do not interact with TA1. We further probed the positioning of these residues in relation to TA1 by sequentially replacing them with Trp. These results indicate that binding becomes progressively worse as the Trp is placed closer to the carboxy terminus (see Fig. 9). Other drastic mutations in this region of C9, including Asp1 and 3 mutated to Asn and Asp1 mutated to Pro, result in no negative affect on binding, further indicating that this region of C9 does not interact directly with TA1, nor does it play a conformational role in C9 presentation to the binding cleft.

Antibody mutations for experimental controls and affinity improvement

Leu30Ala in L1 shows 50% decrease in binding (positive control)

Leu30 falls within a region that defines a canonical loop structure and is directly adjacent to position 29 in L1, which is a primary residue for defining L1 canonical class (Chothia et al., 1989). This mutation demonstrates the degree to which overall binding can be affected by a moderately conservative change (a decrease in side chain volume) in a region that defines loop conformation, even though the position is quite distant from the predicted antigen contact residues (see Fig. 7).

Phe99Tyr in L3 shows a 20% increase in binding (negative control)

Mutations at this position were originally intended to be a negative control by demonstrating that mutation of a residue that was predicted to have no contact with the C9 peptide (see Fig. 7) would have no affect on binding. An Ala mutation showed a 90% drop in binding; however, we felt this effect to be primarily due to a change in the binding site topography caused by the radical de-

crease in side chain volume. We, therefore, tried a more conservative mutation, Tyr. Surprisingly, we saw a 20% increase in binding. Improved binding may be due to a change in the overall L3 structure to increase interface surface area or that the Phe99Tyr, while still maintaining much of the hydrophobic effect, may, in addition, contribute by aromatic hydrogen bonding (Kelley & O'Connell, 1993). This could force C9 into a closer, more favorable binding interface with the L1, L2, and H3 regions.

Tyr213Phe and Tyr218Phe in H3 show binding improvement

Hydrophobic and polar interactions play an important role at the antigen–antibody interface (for review, see Searle et al., 1995). Hydrophobic residues that become buried at the interface cause an increase in solvent entropy, increasing the affinity of the association. Furthermore, two studies (Rini et al., 1992; Schulze-Gahmen et al., 1993) showed that, in the case of an anti-peptide antibody, H3 undergoes a major conformational change during binding. Changing the two Tyr residues in H3 to the more hydrophobic Phe conserved the combining site topography and may have caused H3, upon peptide binding, to associate with Arg9 of C9 with greater surface area contact.

Using binding data from point mutations in the peptide and antibody, we have demonstrated the ability to model a peptide–antibody complex. However, the PENI fusion protein, to which the C9 is connected, could influence some of the binding data. Also, this model can only be used to predict the interactions and side chain positions at the binding interface or identify the possible hydrogen bond-forming residues but cannot define these interactions. Furthermore, the model does not take into account antibody conformational changes that may accompany complex formation, particularly within H3. Therefore, a conclusively accurate model cannot be rendered without the use of X-ray crystallography.

We were able to use the model to identify residues within the TA1 binding cleft and construct mutations that improved the affinity of the antibody for C9. However, we found the rational design of mutations for affinity improvement to be complicated. Several conservative mutations made within the antibody binding site did not perform as anticipated. The process we use here, combining functional studies with modeling methods, enhances the model-based approach to structural study and makes it a viable tool for use in laboratories that do not have access to X-ray crystallographic facilities.

Materials and methods

Construction and purification of C9 mutants using the PENI protein fusion method (R. Tal, C.L. Casipit, V. Wittman, H.C. Wong, in prep.)

Complementary oligonucleotides, containing the C9 coding region, individual mutations, and the umber stop codon were annealed (see Table 2). The annealed oligonucleotides were cloned as

Table 2. *Oligonucleotides used in the mutagenesis of C9*

Mutation	Sequence[a]	Downstream	Upstream
Wild type			
D1A	5′-CCATGGGCATCTGACCGTGCAATCGAAGGTCGTTGAGGGATCC-3′	PKM1-1[b]	PKM1-2
S2A	5′-CCATGGGACGCTGACCGTGCAATCGAAGGTCGTTGAGGGATCC-3′	PKM2-1	PKM2-2
D3A	5′-CCATGGGACTCTGCACGTGCAATCGAAGGTCGTTGAGGGATCC-3′	PKM3-1	PKM3-2
R4A	5′-CCATGGGACTCTGACGCTGCAATCGAAGGTCGTTGAGGGATCC-3′	PKM4-1	PKM4-2
A5S	5′-CCATGGGACTCTGACCGTTCCATCGAAGGTCGTTGAGGGATCC-3′	PKM5-1	PKM5-2
I6A	5′-CCATGGGACTCTGACCGTGCAGCTGAAGGTCGTTGAGGGATCC-3′	PKM6-1	PKM6-2
E7A	5′-CCATGGGACTCTGACCGTGCTATCGCTGGTCGTTGAGGGATCC-3′	PKM7-1	PKM7-2
G8A	5′-CCATGGGACTCTGACCGTGCAATCGAAGCACGTTGAGGGATCC-3′	PKM8-1	PKM8-2
R9A	5′-CCATGGGACTCTGACCGTGCAATCGAAGGTGCATGAGGGATCC-3′	PKM9-1	PKM9-2
AAAAAIAGR	5′-CCATGGGCTGCTGCTGCTGCTATCGCTGGCCGTTGAGGGATCC-3′	AM002	AM001
R9K	5′-CCATGGGACTCTGACCGTGCTATCGAAGGTAAATGAGGGATCC-3′	AM004	AM003
R9I	5′-CCATGGGACTCTGACCGTGCAATCGAAGGTATCTGAGGGATCC-3′	AM006	AM005
E7Q	5′-CCATGGGACTCTGACCGTGCTATCCAGGGTCGTTGAGGGATCC-3′	AM008	AM007
E7D	5′-CCATGGGACTCTGACCGTGCTATCGACGGTCGTTGAGGGATCC-3′	AM010	AM009
E7K	5′-CCATGGGACTCTGACCGTGCAATCAAAGGTCGTTGAGGGATCC-3′	AM012	AM011
I6L	5′-CCATGGGACTCTGACCGTGCACTGGAAGGTCGTTGAGGGATCC-3′	AM016	AM015
I6V	5′-CCATGGGACTCTGACCGTGCAGTTGAAGGTCGTTGAGGGATCC-3′	AM018	AM017
A5G	5′-CCATGGGACTCTGACCGTGGTATCGAAGGTCGTTGAGGGATCC-3′	AM020	AM019
A5C	5′-CCATGGGACTCTGACCGTTGCATCGAAGGTCGTTGAGGGATCC-3′	AM022	AM021
R4K	5′-CCATGGGACTCTGACAAAGCAATCGAAGGTCGTTGAGGGATCC-3′	AM024	AM023
D1&3N	5′-CCATGGAACTCTAACCGTGCAATCGAAGGTCGTTGAGGGATCC-3′	OP002	OP001
D1W	5′-CCATGGTGGTCTGACCGTGCAATCGAAGGTCGTTGAGGGATCC-3′	OP004	OP003
S2W	5′-CCATGGGACTGGGACCGTGCAATCGAAGGTCGTTGAGGGATCC-3′	OP006	OP005
D3W	5′-CCATGGGACTCTTGGCGTGCAATCGAAGGTCGTTGAGGGATCC-3′	OP008	OP007
D1P	5′-CCATGGCCGTCTGACCGTGCAATCGAAGGTCGTTGAGGGATCC-3′	OP010	OP009

[a]Bases that were substituted are underlined.
[b]Downstream and upstream primer designations.

*Nco*I-*Bam*HI cassettes into pCC50. The pCC50 vector is pUC19 containing the PENI gene coding region flanked on the 5′ end by the *Hind*III site and on the 3′ end by *Nco*I/*Bam*HI restriction sites. The resulting plasmids were used to transform strain DG101 (*endA thi1 hsdR supE44 lacI^q lacZΔm15 F$^-$*) obtained from David Gelfand (Roche Molecular Systems, Alameda, California). The PENI–C9 fused genes were then subcloned as *Hind*III-*Bam*HI cassettes into pDG160, a derivative of pFC54.t (Wang et al., 1985), and the resulting plasmids were used to transform strain DG116 (*thi-1 hsdR17 endA1 supE44* [λ cI857 Δ*H1 bioT76*]) obtained from D. Gelfand. Heat induction of the p_L promoter was performed as described elsewhere (Greenfield et al., 1986). The PENI–C9 fusion proteins were purified essentially as described (Johnson et al., 1980; Wittman & Wong, 1988), which included a 35% ammonium sulfate cut followed by monodisperse cation exchange (Mono-S) chromatography (Pharmacia, Uppsala, Sweden). Protein concentrations were determined using the BCA protein assay (Pierce, Rockford, Illinois).

Western Blot analysis

The purified PENI–C9 fusion proteins were loaded at 1ug/well and electrophoresed over a 15% SDS-PAGE. The gel was transferred onto Immobilon (Millipore) membrane using the Semi-dry blotting method (Kyhse-Andersen, 1984). The blot was then blocked for 15 min at room temperature in 1X blotto (9.8 mM $NaPO_4$ pH 7.4, 1% skim milk, 1% NP-40) and was incubated with TA1 diluted in 1X blotto with a final concentration of 2.71 μg/mL for at least 1 h at room temperature. The blot was washed and incubated with 1:10,000 goat anti-mouse IgG HRP (Jackson Immuno Research Laboratories, West Grove, Pennsylvania) diluted in 1X blotto for 30 min at room temperature and then washed and developed with ECL chemiluminescent reagent (Amersham Life Science, Inc., Arlington Heights, Illinois) and exposed to X-ray film for 30 s.

Competition enzyme immunoassay (EIA) analysis

The purified PENI–C9 fusion proteins were assayed for relative binding to the TA1 antibody using a competition EIA. Ninety-six-well microtiter plates (Nunc) were passively coated overnight at 4 °C with 100 ng/well of the PENI–C9(wt). Serial dilutions of the various forms of the PENI–C9 fusion proteins were made in conjugate diluent (19.6 mM Tris-HCl, 244.8 mM NaCl, 0.1% Tween-20, 2% Gelatin) and preincubated for 1 h at room temperature with TA1 (final concentration 271 ng/mL). The coated microtiter plates were washed, 100 μL of each preincubated sample was added to each well, and the plates were incubated for 30 min at room temperature. The plates were washed, 100 μL of 1:2000 goat anti-mouse IgG HRP diluted in conjugate diluent were added to each well, and the plates were incubated for 30 min at room temperature. The plates were washed for a final time, and 100 μL of ABTS substrate (Kirkegaard & Perry Laboratories) was added to each well and allowed to incubate at room temperature for 8 min. The reaction was quenched with 100 μL of 1% SDS stop solution to each well. The signal was then read at 405 nm. Each dilution was performed in triplicate and averaged. The maximum signal (100%) was defined as the signal for PENI preincubated with TA1. The concentration of PENI–C9(wt) preincubated with TA1, which resulted in a signal that was half the maximal signal, was defined as 50% inhibition and all PENI–C9 mutated fusion proteins were compared at this concentration (84 μg/mL).

Biospecific interaction analysis (BIAcore) analysis

The binding affinities of the PENI–C9 fusion proteins to the TA1 monoclonal antibody were analyzed with BIAcore (Pharmacia-Biosensor, Uppsala, Sweden), a biosensor system using surface plasmon resonance detection (Altschuh et al., 1992). TA1 was immobilized onto the surface of a CM5 sensor chip using the amine coupling kit and procedures provided by the manufacturer, which included activation of the sensor chip with 30 μL of a 1:1 mixture of 11.5 mg/mL *N*-hydroxysuccinimide and 75 mg/mL *N*-ethyl-*N*′-(dimethylaminopropyl) carbodimide then injecting 5 μL of TA1 (diluted to 57 μg/mL in 10 mM sodium acetate buffer pH4) at a flow rate of 3 μL/min. Residual dextran binding sites were inactivated by treating the chip surface with 35 μL of 1 M ethanolamine pH 8.5. The resulting TA1 immobilized onto the chip was approximately 4500 resonance units (RU). The purified PENI–C9 fusion proteins were diluted to 30 μg/mL in BIAcore eluent buffer (10 mM HEPES, 150 mM NaCl, 3.4 mM EDTA, 0.005% P20 surfactant, pH 7.4). For each PENI–C9 fusion protein injected, a relative response in RU, representing the amount of PENI–C9 bound, was calculated. Percent of binding was calculated by setting the relative response of PENI–C9(wt) to 100%.

Computer modeling of the antigen–antibody complex

We constructed a model of the TA1 antibody using the Oxford Molecular ABM software (Martin et al., 1989; Rees et al., 1992) on the Silicon Graphics Indigo 2 eXtreme system. The antibody structure was then energy minimized using Biosym Insight II software. We performed an alignment search for the C9 sequence throughout the Brookhaven database without finding any reasonable alignments. Therefore, we constructed the C9 epitope using the Insight II Builder Module to assemble the amino acid sequence in a linear-planar conformation and, based on the binding data from alanine-scan mutagenesis and the binding site constraints of the TA1 model, we created a model of the C9 epitope directionally docked in the TA1 binding cleft using the following procedures: we modified the dihedral angles of the atom bonds along the C9 backbone to allow the epitope to fit within the spatial constraints of the TA1 binding cleft, which we rendered in van der Waals (VDW) surfaces, while also monitoring hydrogen bonding between C9 and TA1. We used translational and rotational movements to position C9 so that hydrogen bonds would be consistently formed between Arg9 in C9 and TA1, while the rest of the C9 peptide would fit within the TA1 binding cleft. At this point, we optimized (a steep sloped energy minimization) the C9 epitope and repositioned it to form the most hydrogen bonds, less than or equal to 2 Å, with TA1 while minimizing bumping to ensure that C9 was not penetrating any VDW surfaces on the TA1 cleft. We then energy minimized the C9 epitope, which yielded little change to the overall conformation.

Site-specific mutatgenesis, expression, and purification of TA1

To construct and express the TA1(wt) and mutated antibodies, we used a set of cloned anti-digoxin IgG_{2B} heavy-chain (HC) and κ light-chain (LC) antibody gene vectors (generously provided by Richard I. Near) and a mammalian cell antibody transfection and expression protocol (Near et al., 1990). The vectors were altered via site-directed mutagenesis so that the anti-digoxin heavy and light chain F_V coding regions could be replaced with

Table 3. *Oligonucleotides used in the mutagenesis of TA1*

Mutation	Sequence of spanned region[a]	Downstream	Upstream
W164A	5′-GGCCTGGAGTGGATTGGAGCGATTGATCCTGATAATGGT-3′	[b]	CLC354
Y213A	5′-GTCTATTACTGTGACTACGCTAGGTTCGACGACTATGCT-3′	[b]	CLC355
Y37A	5′-CATAGTAATGGCAACACTGCCTTGTATTGGTTCCTGCAG-3′	CLC347	CLC356
R55A	5′-CCTCAGCTCCTGATATATGCGATGTCCAACCTTGCCTCA-3′	CLC348	CLC357
H96A	5′-GTTTATTACTGTTTTGCAGGCTCTAGAATTTCCGCTCACG-3′	CLC349	CLC358
F99W	5′-TGTTTGCAGCATCTAGAATGGCCGCTCACGTTCGGTGCT-3′	CLC350	CLC359
F99A	5′-TGTTTGCAGCATCTAGAAGCTCCGCTCACGTTCGGTGCT-3′	CLC351	CLC360
Y213F	5′-TGTGACTACTTCAGGTTCGAC-3′	CLC390	CLC391
W164Y	5′-TGGATTGGATATATTGATCTT-3′	CLC392	CLC393
R55K	5′-CTGATATATAAGATGTCCAAC-3′	CLC394	CLC395
Y37F	5′-GGTAACACTTTCTTGTATTGG-3′	CLC396	CLC397
L30A	5′-AAGAGTCTCGCTCATAGTAAT-3′	CLC398	CLC399
F99Y	5′-CATCTAGAATATCCGCTCACG-3′	CLC400	CLC401
Y218F	5′-TTCGACGACTTCGCTGTGGAC-3′	LDE001	LDE002

[a]Bases that were substituted are underlined.
[b]These mutations were created by site-specific mutagenesis.

the TA1 HC and LC F_V functional genes (see Fig. 11 for vector diagrams).

Overlapping PCR (Horton et al., 1989) was used to create the specific mutations within the complimentarity determining regions (CDR) of TA1. Primers that spanned the codon sequences to be mutated were synthesized (see Table 3). The resulting PCR products were cloned as EcoRV-EagI cassettes into the modified anti-digoxin IgG_{2B} HC and κ LC gene vectors. The resulting plasmids were used to transform strain XL1 blue (*endA hsdR− HsdM+ lacZΔm15 recA lacI^q F′*). The final constructs containing TA1 VH or VL functional regions with flanking constant and intron splicing regions were then subcloned in correct orientation as XbaI cassettes (for HC) or EcoRI/XbaI cassettes (for LC) into pSVgpt/26-10VH or pneo/26-10VL, respectively. The resulting plasmids were used to transform strain DG103 (*endA thi1 hsdR supE44 lacI^q lacZΔm15 F⁻ dam13::Tm9*) obtained from D. Gelfand. Ten micrograms of each plasmid was linearized with EcoRI and transfected into 1×10^7 Nso cells in 0.8 mL PBS by electroporation at 250 V and 960 uFD. After 24 h the transfected cells were placed under selective growth media: 1.2 μg/mL mycophenolic acid and 1X hypoxanthine (for HC) or 1.2 mg/mL G418 (for LC). Resulting colonies were screened for IgG_{2B} or κ chain expression. Those that were positive were expanded and cotransfected with the TA1 IgG_{2B}(wt) or κ chain(wt) counterpart and screened for IgG_{2B} and κ chain production. Positive colonies were expanded and the antibodies were purified by Protein A affinity chromatography from conditioned media and assayed by BIAcore and EIA.

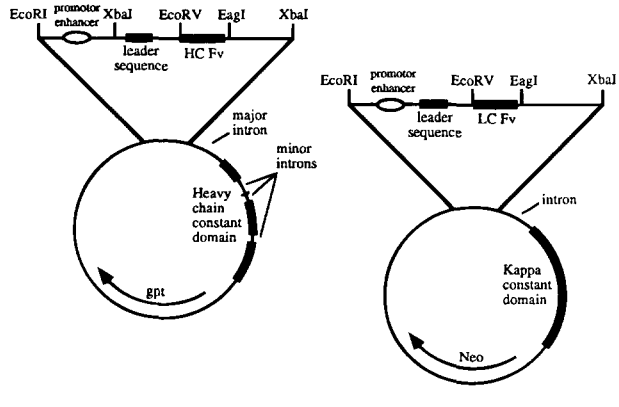

Fig. 11. Plasmid vectors used to construct the TA1 HC and LC F_V regions. Physical maps of the heavy- and light-chain vectors used to clone the TA1 HC and LC F_V PCR products within the EcoRV and EagI restriction sites and transfect NS0 cells; gpt, geneticin (G418) resistance gene; Neo, neomycin resistance gene.

Acknowledgments

We thank Dr. Keith Brew for reviewing the manuscript and providing valuable and essential comments, Effrain Venezuela for performing the nucleotide sequencing analysis, Elizabeth Thomson for providing the oligonucleotides used in this work, Bee Huang for technical computer support, and Aleyda Mejia and Obdulio Piloto for their help with the PENI–C9 mutants.

References

Altschuh D, Dubs M, Weiss E, Zeder-Lutz G, Van Regenmortel MHV. 1992. Determination of kinetic constants for the interaction between a monoclonal antibody and peptides using surface plasmon resonance. *Biochemistry 31*:6298–6304.

Amit AG, Mariuzza RA, Phillips SEV, Poljak RJ. 1986. Three-dimensional structure of an antigen–antibody complex at 2.8 Å resolution. *Science 233*:747–753.

Ban N, Escoban C, Garcia R, Hasel K, Day J, Greenwood A, McPherson A. 1994. Crystal structure of an idiotype–anti-idiotype Fab complex. *Proc Natl Acad Sci USA 91*:1604–1608.

Bentley GA, Boulot G, Riottot MM, Poljak RJ. 1990. Three-dimensional structure of an idiotype–anti-idiotype complex. *Nature 348*:254–257.

Braden BC, Souchon H, Eisele JL, Bentley GA, Bhat TN, Navaza J, Poljak RJ. 1994. Three-dimensional structures of the free and the antigen-complexed Fab from monoclonal anti-lysozyme antibody D44.1. *J Mol Biol 243*:767–781.

Braden BC, Poljak RJ. 1995. Structural features of the reactions between antibodies and protein antigens. *FASEB J 9*:9–16.

Bruccoleri RE, Heuber E, Novotny J. 1988. Structure of antibody hypervariable loops reproduced by a conformational search algorithm. *Nature 335*:564–568.

Brunger AT, Leahy DJ, Hynes TR, Fox RO. 1991. 2.9 Å resolution structure of an anti-dinitrophenyl-spin-label monoclonal antibody Fab fragment with bound hapten. *J Mol Biol 221*:239–256.

Chothia C, Lesk AM, Tramontano A, Levitt M, Smith-Gill SJ, Ain G, Sheriff S, Padlan EA, Davies D, Tulip WR, Colman PM, Spinelli S, Alzani PM, Poljak RJ. 1989. Conformations of immunoglobulin hypervariable regions. *Nature 342*:877–883.

Creighton TE. 1993. Electrostatic forces. In: *Proteins structures and molecular properties*, 2nd ed. New York: W. H. Freeman and Company. pp 142–145.

Degan S, MacGillivray R, Davie E. 1983. Characterization of the complementary deoxyribonucleic acid and gene coding for human prothrombin. *Biochemistry 22*:948–954.

de la Paz P, Sutton J, Darsley MJ, Rees AR. 1986. Modeling of the combining sites of three anti-lysozyme monoclonal antibodies and of the complex between one of the antibodies and its epitope. *EMBO J 5*:415–425.

Dyson HJ, Wright PE. 1995. Antigenic peptides. *FASEB J 9*:37–42.

Evans SV, Rose DR, To R, Young NM, Bundle DR. 1994. Exploring the mimicry of polysaccharide antigens by anti-idiotypic antibodies The crystallization, molecular replacement, and refinement to 2.8 Å resolution of an idiotope–anti-idiotope Fab complex and of the unliganded anti-idiotope Fab. *J Mol Biol 241*:691–705.

Greenfield L, Dovey H, Lawyer F, Gelfand D. 1986. High-level expression of diphtheria toxin peptides in *Escherichia coli*. *Biotechnology 4*:1006–1011.

Herron JN, He XM, Ballard DW, Blien PR, Pace PE, Bothwell AL, Voss EW Jr, Edmundson AB. 1991. An autoantibody to single-stranded DNA: Comparison of the three-dimensional structures of the unliganded Fab and a deoxynucleotide–Fab complex. *Proteins 11*:159–175.

Herron JN, He X, Mason EL, Voss EW Jr, Edmundson AB. 1989. Three dimensional structure of a fluorescein–Fab complex crystallized in 2-methyl-2,4-pentanediol. *Proteins 5*:271–280.

Horton RM, Hunt HD, Ho SN, Pullen JK, Pease LR. 1989. Engineering hybrid genes without the use of restriction enzymes: Gene splicing by overlap extension. *Gene 77*:61–68.

Jeffrey GA, Saenger W. 1991. Hydrogen bonding in amino acids and peptides: Predominance of Zwitterions. In: *Hydrogen bonding in biological structures*. Berlin: Springer Verlag. pp 351–393.

Johnson AD, Pabo CO, Sauer RT. 1980. Bacteriophage l repressor and cro protein: Interactions with operator DNA. *Methods Enzymol 65*:839–855.

Kelley RF, O'Connell MP. 1993. Thermodynamic analysis of an antibody functional epitope. *Biochemistry 32*:6828–6835.

Kyhse-Andersen J. 1984. Electroblotting of multiple gels: A simple apparatus without buffer tank for rapid transfer of proteins from polyacrylamide to nitrocellulose. *J Biochem Biophys Methods 10*:203–209.

Laskowski RA, MacArthur MW, Moss DS, Thornton JM. 1993. PROCHECK: A program to check the stereochemical quality of protein structures. *J Appl Crystallogr 26*:283–291.

Martin ACR, Cheetham JC, Rees AR. 1989. Modeling antibody hypervariable loops: A combined algorithm. *Proc Natl Accad Sci USA 86*:9268–9272.

Near RI, Mudgett-Hunter M, Novotny J, Bruccoleri R, Ng SC. 1993. Characterization of an anti-digoxin antibody binding site by site-directed in vitro mutagenesis. *Mol Immun 30*:369–377.

Near RI, Ng SC, Mudgett-Hunter M, Hudson NW, Margolies MN, Seidman JG, Haber E, Jacobson MA. 1990. Heavy and light chain contributions to antigen binding in an anti-digoxin chain recombinant antibody produced by transfection of cloned anti-digoxin antibody genes. *Mol Immun 27*:901–909.

Rees AR, Martin ACR, Pedersen JT, Searle SMJ. 1992. *ABM™, a computer program for modeling variable regions of antibodies*. Oxford, UK: Oxford Molecular Ltd.

Rini JM, Schulze-Gahmen U, Wilson IA. 1992. Structural evidence for induced fit as a mechanism for antibody-antigen recognition. *Science 255*:959–965.

Roberts S, Cheetham JC, Rees AR. 1987. Generation of an antibody with enhanced affinity and specificity for its antigen by protein engineering. *Nature 328*:731–734.

Ruff-Jamison S, Glenney JR Jr. 1993. Molecular modeling and site-directed mutagenesis of an anti-phosphotyrosine antibody predicts the combining site and allows the detection of higher affinity interactions. *Protein Eng 6*:661–668.

Schulz GE, Schirmer RH. 1979. Side chain properties. In: *Principles of protein structure*. New York: Springer Verlag. pp 10–14.

Schulze-Gahmen U, Rini JM, Wilson IA. 1993. Detailed analysis of the free and bound conformations of an antibody X-ray structures of Fab 17/9 and three different Fab-peptide complexes. *J Mol Biol 234*:1098–1118.

Searle SJ, Pedersen JT, Henry AH, Webster DM, Rees AR. 1995. Antibody structure and function. In: Borrebaeck CAK, ed. *Antibody engineering*, 2nd ed. New York: Oxford University Press. pp 3–51.

Stanfield RL, Fieser TM, Lerner RA, Wilson IA. 1990. Crystal structures of an antibody to a peptide and its complex with peptide antigen at 2.8 Å. *Science 248*:712–719.

Strong RK, Campbell R, Rose DR, Petsko GA, Sharon J, Margolies MN. 1991. Three-dimensional structure of murine anti-p-azophenylarsonate Fab 36-71. 1. X-ray crystallography, site-directed mutagenesis, and modeling of the complex with hapten. *Biochemistry 30*:3739–3748.

Totrov M, Abagyan R. 1994. Detailed *ab initio* prediction of lysozyme-antibody complex with 1.6 Å accuracy. *Struct Biol 1*:259–263.

Verdaguer N, Mateu MG, Andreu D, Giralt E, Domingo E, Fita I. 1995. Structure of the major antigenic loop of foot-and-mouth disease virus complexed with a neutralizing antibody: Direct involvement of the Arg-Gly-Asp motif in the interaction. *EMBO J 14*:1690–1696.

Walls PH, Sternberg JE. 1992. New algorithm to model protein–protein recognition based on surface complementarity: Applications to antibody–antigen docking. *J Mol Biol 228*:277–297.

Wang A, Creasey A, Ladner MB, Lin LS, Strickler J, van Arsdell JN, Yamamoto R, Mark DF. 1985. Molecular cloning of the complementary DNA for human tumor necrosis factor. *Science 228*:149–154.

Wang D, Ligo J, Mitra D, Akolkar D, Gruezo F, Kabat B. 1991. The repetoire of antibodies to a single antigenic determinant. *Mol Immunol 28*:1387–1397.

Wittman V, Wong HC. 1988. Regulation of the penicillinase genes of *Bacillus licheniformis*: Interaction of the *pen* repressor with its operators. *J Bacteriol 170*:3206–3212.